Electrocatalysis

Deutsche Ausgabe: DOI: 10.1002/ange.201411626
Internationale Ausgabe: DOI: 10.1002/anie.201411626

Recycling Application of Li–MnO_2 Batteries as Rechargeable Lithium–Air Batteries**

Yuxiang Hu, Tianran Zhang, Fangyi Cheng, Qing Zhao, Xiaopeng Han, and Jun Chen**

Abstract: *The ever-increasing consumption of a huge quantity of lithium batteries, for example, Li–MnO_2 cells, raises critical concern about their recycling. We demonstrate herein that decayed Li–MnO_2 cells can be further utilized as rechargeable lithium–air cells with admitted oxygen. We further investigated the effects of lithiated manganese dioxide on the electrocatalytic properties of oxygen-reduction and oxygen-evolution reactions (ORR/OER). The catalytic activity was found to be correlated with the composition of Li_xMnO_2 electrodes ($0 < x < 1$) generated in situ in aprotic Li–MnO_2 cells owing to tuning of the Mn valence and electronic structure. In particular, modestly lithiated $Li_{0.50}MnO_2$ exhibited superior performance with enhanced round-trip efficiency (ca. 76%), high cycling ability (190 cycles), and high discharge capacity (10823 mA h g_{carbon}^{-1}). The results indicate that the use of depleted Li–MnO_2 batteries can be prolonged by their application as rechargeable lithium–air batteries.*

Lithium batteries have widespread application and dominate the current battery market.[1] Among them, Li–MnO_2 batteries are viable for large-scale deployment, for example, in the areas of portable electronics and medical devices, owing to their high capacity, nontoxicity, and high resource abundance. As their annual production reaches hundreds of millions, one can expect a huge amount of depleted cells,[2] which require complex, costly, and energy-consuming methods for retrieval.[3] Meanwhile, conventional Li–MnO_2 cells (ca. 250 Wh kg^{-1}) could hardly satisfy the increasing demand of energy density; alternatively, rechargeable lithium–air or Li–O_2 batteries theoretically offer a several-fold higher energy content (> 3500 Wh kg^{-1}) but are impeded by critical issues, such as sluggish oxygen-reduction/evolution reactions (ORR/OER).[4] Manganese dioxide could act not only as the cathode material in Li–MnO_2 batteries, but also as a catalyst to enhance the electrocatalytic activity of rechargeable Li–O_2 cells.[5,6] The similar cell structure and components (cathode, lithium anode, separator, and organic electrolyte) of aprotic Li–MnO_2 batteries and rechargeable Li–O_2 batteries (with a MnO_2 electrode) encouraged us to investigate whether decayed Li–MnO_2 cells could be utilized directly as high-capacity rechargeable Li–air batteries with an active mass of admitted oxygen. To the best of our knowledge, the concept of the direct and dual utilization of the depleted electrodes in Li–MnO_2 cells has not been reported previously. Furthermore, the discharge of manganese oxide electrodes in Li–MnO_2 cells enables in situ electrochemical tuning of manganese oxide catalysts, which generally suffer from low catalytic activity and poor electrical conductivity.[7] Recent studies have shown that the delithiation of lithium–metal oxides (e.g., $LiCoO_2$ or $LiMn_2O_4$) can adjust their electronic structures and enhance their ORR/OER activity in aqueous electrolytes.[8,9] However, such an effect remains unclear in the non-aqueous media commonly employed in Li–O_2 battery systems.

Herein, we demonstrate that after their depletion, sealed Li–MnO_2 cells with manganese oxides as the cathode can be operated efficiently as rechargeable Li–air batteries when the cathode is exposed to air or oxygen. Similar characteristics of dual applicability were identified in other prevailing cathode materials, such as $LiCoO_2$ and $LiFePO_4$. We further disclose that the electrocatalytic properties for ORR/OER correlate with the degree of lithiation of MnO_2. As compared to the pristine oxide, the lithiated electrode exhibits improved catalytic activity, thus resulting in lower discharge/charge overvoltage, larger capacity, and better rate capability. In particular, $Li_{0.50}MnO_2$ delivers high energy efficiency (ca. 76%) and durable cyclability (over 190 cycles) in Li–O_2 batteries.

Pristine MnO_2 was synthesized by replicating mesoporous silica[10] and featured interconnected nanosized pores and a high surface area (see Figure S1 in the Supporting Information). These properties should benefit electrolyte immersion, Li^+ transport, and gas diffusion for the oxygen electrode. We coupled the prepared mesoporous MnO_2 with an Li anode to assemble Li–MnO_2 cells with an organic electrolyte of 1M lithium bis(trifluoromethanesufonyl)imide (LiTFSI) in tetraethyleneglycol dimethyl ether (TEGDME). The positive side of the cells was predrilled with homogenously distributed holes. These holes were covered by a gas-impermeable membrane and were exposed to O_2 or air to create rechargeable Li–O_2 or Li–air batteries (Figure 1, inset). In the cathode, MnO_2 was mixed with carbon in a weight ratio of 1:2 to ensure sufficient electrical conductivity.

Figure 1a displays the galvanostatic charge–discharge profiles of the sealed Li–MnO_2 cell. At a current density of 154 mA $g_{MnO_2}^{-1}$ (equivalent to 77 mA g_{carbon}^{-1}, corresponding to 0.5 C), a capacity retention of 74% was attained after

[*] Y. Hu,[+] T. Zhang,[+] F. Cheng, Q. Zhao, X. Han, J. Chen
Key Laboratory of Advanced Energy Materials Chemistry (Ministry of Education), Collaborative Innovation Center of Chemical Science and Engineering, Nankai University
Tianjin 300071 (China)
E-mail: fycheng@nankai.edu.cn
chenabc@nankai.edu.cn

[+] These authors contributed equally.

[**] We gratefully acknowledge the Programs of National 973 (2011CB935900), the NSFC (21231005 and 21322101), and the MOE (B12015 and ACET-13-0296).

Supporting information for this article is available on the WWW under http://dx.doi.org/10.1002/anie.201411626.

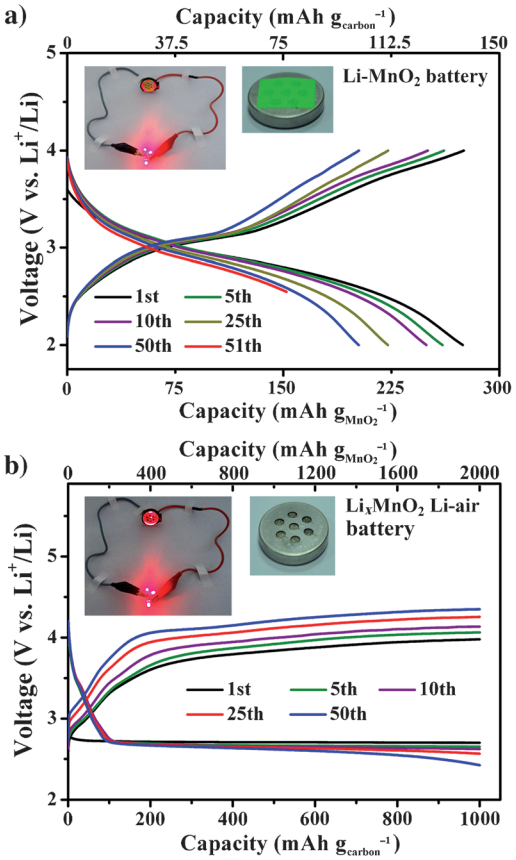

Figure 1. Discharge and charge curves of mesoporous MnO_2-based electrodes in a) a Li–MnO_2 battery and b) a Li–air cell. The Li–MnO_2 cell was cycled between 2.0 and 4.0 V for 50 cycles and ceased to a discharged state of $Li_{0.50}MnO_2$. The same cell was then exposed to air and was discharged/charged at a current density of 100 mA g_{carbon}^{-1}. Insets show photographs of the assembled batteries powering light-emitting diodes.

50 cycles. The electrode was discharged to a cutoff capacity of 154 mAh $g_{MnO_2}^{-1}$ (equivalent to 77 mAh g_{carbon}^{-1}) to give a nominal composition of $Li_{0.50}MnO_2$. After air was admitted through the predrilled holes, the cell became a lithium–air system. This cell could continuously operate for up to 50 cycles at a current density of 100 mA g_{carbon}^{-1} (Figure 1b). The results were encouraging despite a gradual polarization increase in ambient air. As both Li–MnO_2 and Li–air batteries presented herein share the same cell structure and components, dual application of the MnO_2 electrodes is possible. More importantly, the results confirm that cycled metal-oxide-based lithium batteries can be subsequently utilized as rechargeable lithium–air batteries to gain additional cycling use. Notably, even at an intentionally high loading of the active mass, the energy output of the total Li–O_2 cell was 1.6-fold that of the parent Li–MnO_2 cell, although the harvested energy density (160 Wh kg^{-1}) leaves much room for further improvement (see Figure S2 and Table S1 in the Supporting Information). The full cell energy/capacity ratio of Li–O_2 to Li–MnO_2 increased as the mass loading was lowered (see Table S2). Furthermore, our preliminary investigations indicate that the recycling utilization of cycled electrodes can be extended to other common cathode materials, such as $LiCoO_2$ and $LiFePO_4$. Both Li–$LiCoO_2$ and Li–$LiFePO_4$ cells could deliver remarkably high capacities after 100 cycles when oxygen was admitted (see Figures S3 and S4).

Next, it was important to study the lithium content in Li_xMnO_2. Thus, we evaluated the effect of electrochemical lithiation on the catalytic performance of metal oxides in an aprotic electrolyte. The mesoporous MnO_2 electrode was discharged to different ending states in Li–MnO_2 cells (Figure 2a). By controlling the discharge capacity, five representative samples were obtained, namely, MnO_2, $Li_{0.25}MnO_2$, $Li_{0.50}MnO_2$, $Li_{0.75}MnO_2$, and $Li_{0.92}MnO_2$. Figure 2b shows the X-ray diffraction (XRD) patterns of the synthesized Li_xMnO_2 samples. In addition to peaks associated with the carbon additive, there is a characteristic peak at around $2\theta = 37°$, which can be indexed to the (101) plane of β-MnO_2 (JCPDS card no. 24-735). No phase transformation occurred on discharging MnO_2. However, as the discharge proceeded, the (101) peak shifted to a lower diffraction angle (Figure 2b, inset), thus suggesting expansion of the interplanar spacing as a result of Li insertion. Furthermore, the Mn $2p_{3/2}$ peak in the X-ray photoelectron spectrum moved towards a lower binding-energy position upon gradual discharging of MnO_2 (Figure 2c; see also Figure S5). This result confirms the expected reduction of the Mn valence (from about 4 to about 3) owing to Li uptake.[9a] The morphology and structure of Li_xMnO_2 were further characterized by scanning/transmission electron microscopy (SEM/TEM; Figure 2d–g; see also Figures S6 and S7). Despite slight lattice dilation, the nanoporous structure and crystallinity of the oxides were essentially preserved during the lithiation process.

The electrochemical performance of Li_xMnO_2 ($x = 0$, 0.25, 0.50, 0.75, and 0.92) electrodes generated in situ in Li–MnO_2 cells was then investigated for rechargeable Li–O_2 batteries. The electrodes were simply exposed to oxygen for direct use, without the need for complicated posttreatment (e.g., cell disassembly and repeated washing[8]), which is normally required in electrochemical synthesis. Figure 3a shows the initial discharge/charge profiles of the cells based on Li_xMnO_2 electrodes with a cutoff capacity of 1000 mA h g_{carbon}^{-1}. The voltage plateau varied with the composition of Li_xMnO_2 (Figure 3b). For the charge process, the overpotentials on the lithiated MnO_2 were much lower than that on the pristine MnO_2, thus indicating significantly enhanced OER catalytic activity as a result of lithiation. This enhancement increased with increasing lithium content in Li_xMnO_2. For the discharge process, the overvoltage of the electrodes decreased in the order $Li_{0.50}MnO_2 > Li_{0.75}MnO_2 > Li_{0.25}MnO_2 > Li_{0.92}MnO_2 > MnO_2$, thus implying superior ORR activity of lithiated oxides. Remarkably, $Li_{0.50}MnO_2$ enables a voltage separation of 0.87 V between the discharge and charge plateaus, which results in a round-trip efficiency of approximately 76%. This value is 13% higher than that of pristine MnO_2 and is comparable to the results reported for platinum-based catalysts (see Table S3).[11] In the case of $LiCoO_2$ and $LiFePO_4$ electrodes, we also found a composition-dependent electrocatalytic effect. Half-delithiated cathodes resulted in the lowest ORR/OER overpotentials (see Figure S4).

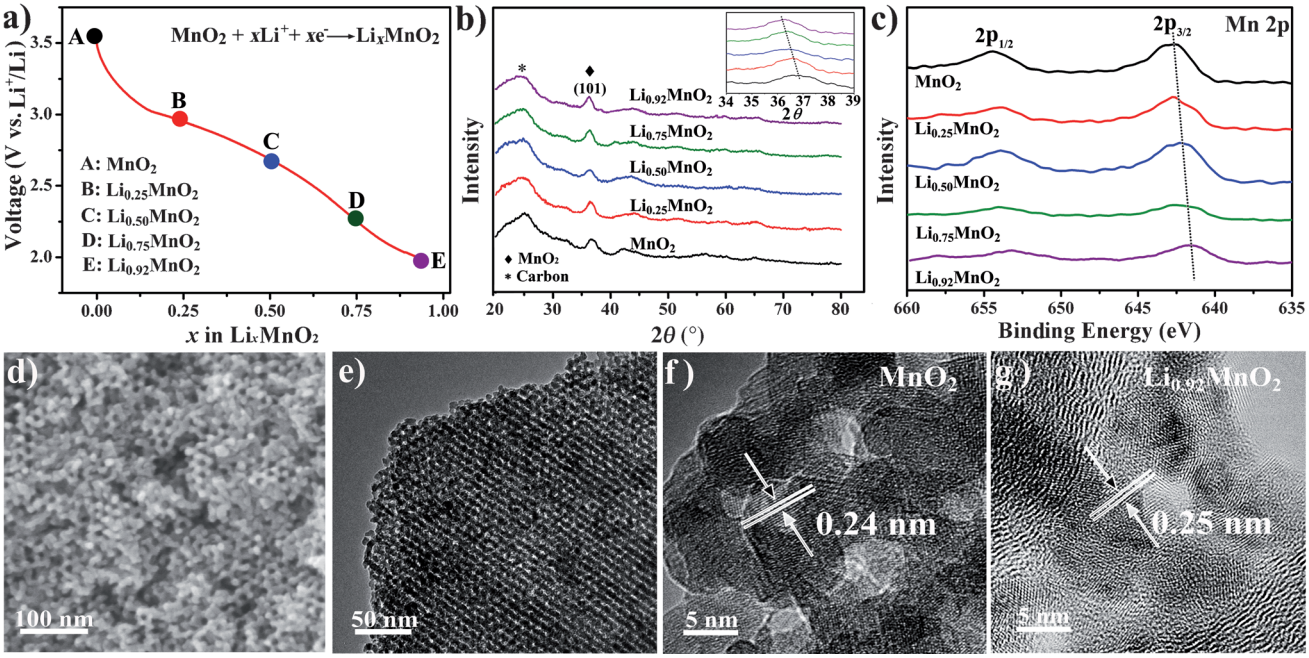

Figure 2. a) A typical discharge curve of MnO_2. Points A, B, C, D, and E mark the representative Li_xMnO_2 species ($x = 0$, 0.25, 0.50, 0.75, and 0.92). b) XRD patterns of the electrodes as collected at the discharged states of Li_xMnO_2 ($x = 0$, 0.25, 0.50, 0.75, and 0.92). The inset shows an enlargement the MnO_2-related peaks. c) Mn 2p XPS spectra of Li_xMnO_2 electrodes ($x = 0$, 0.25, 0.50, 0.75, 0.92). d) SEM and e) TEM images of the pristine mesoporous MnO_2. f,g) HRTEM images of Li_xMnO_2 ($x = 0$ and 0.92).

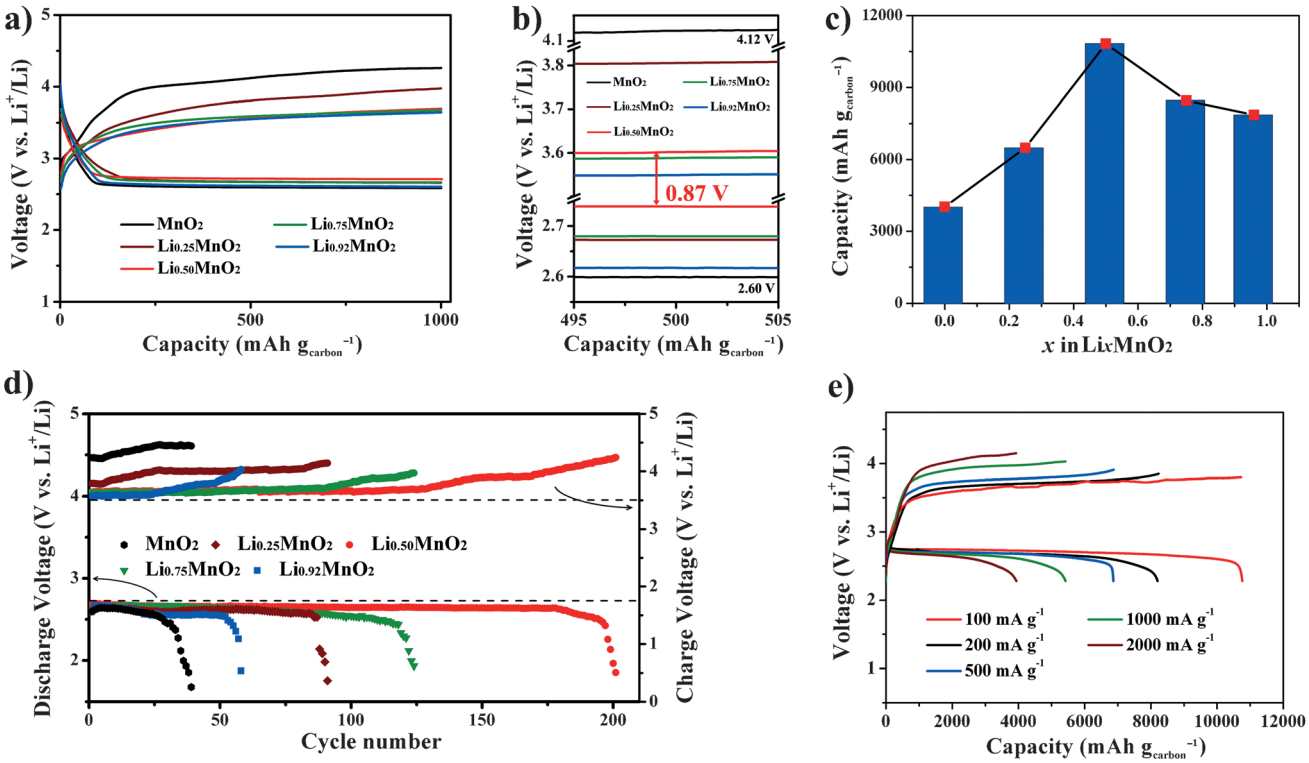

Figure 3. a) First-cycle voltage profiles of the five Li_xMnO_2-based Li–O_2 batteries at a current density of 100 mA g_{carbon}^{-1}. b) Comparison of the discharge–charge overpotentials of the curves displayed in (a). The color coding is the same as in (d). c) Discharge capacities at 100 mA g_{carbon}^{-1} with a cutoff voltage of 2.2 V. d) Terminal discharge/charge voltage versus cycle number at 200 mA g_{carbon}^{-1} and a controlled capacity of 1000 mAh g_{carbon}^{-1}. e) Rate capability of the $Li_{0.50}MnO_2$-based cell at different current densities.

Figure 3c shows the capacities of the Li_xMnO_2 cells discharged to an ending voltage of 2.2 V. As compared with the pristine oxide electrode, all lithiated electrodes delivered much larger capacities. The highest value of 10823 mAh g_{carbon}^{-1} was observed for $Li_{0.50}MnO_2$. The cycling stability of rechargeable Li–O_2 cells is shown in Figure 3d. The cell with the $Li_{0.50}MnO_2$ electrode operated for 197 cycles with a stable terminal discharge voltage above 2 V and a terminal charge voltage below 4.5 V, thus exceeding the operating lifetime of other electrodes (i.e., 148, 90, 57, and 43 cycles for $Li_{0.75}MnO_2$, $Li_{0.25}MnO_2$, $Li_{0.92}MnO_2$, and MnO_2, respectively). Additionally, the $Li_{0.50}MnO_2$ cell exhibited considerable rate capability, although the discharge/charge polarization increased at higher current densities (Figure 3e). In rate-performance tests, the ending charge capacities were set to fit the discharge capacity to avoid overcharging. A discharge capacity of about 4000 mAh g_{carbon}^{-1} was attained even at a high current density of 2000 mA g_{carbon}^{-1}. Moreover, the open-circuit voltage of the Li–O_2 cell based on the $Li_{0.50}MnO_2$ cathode was quite stable in oxygen within an ageing time of 390 h (see Figure S8a). The discharge capacity of the aged electrode was 94% that of the fresh electrode (see Figure S8b). The results suggest that the cell undergoes self-discharge but only to a small extent. Furthermore, the XRD patterns of the electrodes (see Figure S9) indicate no discernable formation of lithium oxides at the anode during extended cycling in O_2.

The $Li_{0.50}MnO_2$ electrode was dismantled from the Li–O_2 cell and analyzed at different discharged/charged states. Both Raman spectra and XRD patterns proved the efficient formation of Li_2O_2 on discharging and the decomposition of Li_2O_2 on charging (see Figure S10). Reversible generation and oxidation of Li_2O_2 is generally viewed as the key to the successful operation of a Li–O_2 battery.[12,13] The superior ability of $Li_{0.50}MnO_2$ to promote the complete decomposition of the insulating peroxide was evidenced by electrochemical impedance spectroscopy (EIS), which showed good recovery of charge–transfer resistance on recharge (see Figure S11). Although $Li_{0.50}MnO_2$ is dischargeable at the tested working voltage range even in an Ar atmosphere, this behavior contributes negligibly to the overall capacity of the Li–O_2 cell (see Figure S12). A previous study also showed that discharged electrode materials could be chemically oxidized in the presence of oxygen.[14] Thus, the lithiated manganese oxide itself could be electrochemically active; redox reactions of 3d metal oxides have been suggested to mediate the process of oxygen electrocatalysis.[9,15] Notably, the XRD profile, the Mn 2p XPS spectrum, and the neighboring layer distance in TEM images were almost unchanged after cycling (see Figure S13), thus indicating respectable stability of the $Li_{0.50}MnO_2$ catalyst.

To understand the enhanced catalytic performance of lithiated MnO_2, we performed density functional theory (DFT) calculations, which are an effective tool for the study of the electrochemical properties of manganese oxides.[16] Our preliminary results reveal a change in electronic structure after lithiation (see Figure S14). For pristine MnO_2, there was a clear band gap near the Fermi level in the density-of-state (DOS) profile, in agreement with its typical semiconductive nature.[16a] However, for $Li_{0.50}MnO_2$, the gap is significantly smaller, which implies better electronic conduction and would favor charge transfer during electrochemical reactions. Alteration of the electron structure was also reported for other Li_xMnO_2 samples.[16c] A comparison of the calculated adsorption energy of Li (5.44 eV) and O_2 (0.079 eV) on the MnO_2 surface shows that Li is attached first to the surface. The result coincides with those of previous DFT modeling, which showed that the initial reduction of oxygen occurs more favorably by the dissociative adsorption of O_2 at the lithiated MnO_2 surface.[16d] O_2 binds significantly more strongly and the O–O bond is elongated to a greater extent on the lithiated oxide surface as compared to the lithium-free surface owing to a different mode of adsorption and an extra Li–O interaction (see Figure S15). The calculated energies of O_2 absorption on MnO_2, $Li_{0.50}MnO_2$, and $LiMnO_2$ are 0.079, 1.171, and 3.279 eV, respectively. Since a good oxygen electrocatalyst should not interact with O_2 too weakly or too strongly, $Li_{0.50}MnO_2$ with a modest oxygen-binding energy showed the highest ORR activity. For the OER process, previous studies have demonstrated that an Mn^{III} oxide with an e_g occupancy near 1 is most favorable,[17] which could explain the lowest charging overpotential of $Li_{0.92}MnO_2$ with a nominal Mn valence of 3.08. Therefore, electrochemical lithiation benefits the ORR/OER on manganese oxide by tuning its electronic properties, surface structure, and oxidation state. Further DFT studies on the reaction mechanism with lithium superoxide/peroxide species are under way.

In conclusion, we have reported that a manganese oxide cathode can first operate in a Li–MnO_2 battery and subsequently serve as efficient catalyst for a rechargeable Li–air battery when oxygen is admitted. Mesoporous MnO_2 lithiated in situ in a Li–MnO_2 cell shows composition-dependent electrocatalytic performance for the ORR/OER in a non-aqueous electrolyte. Remarkably, the $Li_{0.50}MnO_2$ electrode exhibited higher capacity, lower charge–discharge overpotentials, and better cyclability in comparison with the pristine oxide. The present study not only indicates the promising recycling use of depleted Li–MnO_2 batteries as high-energy rechargeable lithium–air batteries, but also sheds light on the electrochemical tuning of transition-metal-oxide electrocatalysts.

Experimental Section

Pristine mesoporous MnO_2 was synthesized by structure replication by using silica KIT-6 as a template. In a typical synthesis, mesoporous KIT-6 (0.5 g; JCNANO) was dispersed in an aqueous solution of $Mn(NO_3)_2$ (6.0 g, 50 wt%; Aladdin). The mixture was stirred overnight, and then filtered and dried at 80°C. The obtained powder was calcined at 400°C for 3 h in air, and then treated with 2 M aqueous KOH at 60°C to remove the KIT-6 silica template. The resulting mixture was filtered and repeatedly washed with distilled water. The mesoporous MnO_2 was obtained after drying at 80°C under vacuum for 4 h.

Lithiated mesoporous MnO_2 (Li_xMnO_2) was prepared by an in situ electrochemical discharge route. First, the synthesized pristine mesoporous MnO_2 was mixed with Super P carbon and poly(vinylidene fluoride) (PVdF) binder in the solvent *N*-methyl-2-pyrrolidone (NMP) in a weight ratio of 3:6:1. The mixture was pasted on a nickel-foam current collector to form the working electrode, which was dried

at 110 °C under vacuum for 6 h. The electrolyte was 1 M LiTFSI in TEGDME, and the separator was glass fiber. The prepared working electrodes were coupled with lithium-foil counter electrodes to assemble the CR-2032 coin-type lithium cells in an argon-filled glove box (Mikrouna Universal 2440/750). The cathode cap was predrilled with seven homogenously distributed holes, which would be used to import oxygen later. For the synthesis of lithiated mesoporous MnO_2 (Li_xMnO_2), the as-assembled cells were discharged at a current density of 154 mA $g_{MnO_2}^{-1}$ (equivalent to 77 mA g_{carbon}^{-1}) to the desired ending states by controlling the discharge capacity. The composition of MnO_2, $Li_{0.25}MnO_2$, $Li_{0.50}MnO_2$, $Li_{0.75}MnO_2$, and $Li_{0.92}MnO_2$ corresponds to discharging to a cutoff capacity of 0, 77, 154, 231, and 283 mAh $g_{MnO_2}^{-1}$ (equivalent to 0, 38.5, 77, 115.5, and 141.5 mAh g_{carbon}^{-1}), respectively.

The synthesized materials and cycled electrodes were characterized by SEM (JEOL JSM7500F, accelerating voltage 5 kV), TEM (Philips Tecnai F20, accelerating voltage 200 kV), XRD (MiniFlex600 X-ray generator, copper source, Kα radiation), and confocal Raman microscopy (DXR, ThermoFisher Scientific, excitation at 532 nm by an argon-ion laser). X-ray photoelectron spectra were collected on a PerkinElmer PHI 1600 ESCA system. The Brunauer–Emmett–Teller (BET) specific surface area was measured by N_2 adsorption–desorption at 77 K with a BELSORP-Mini instrument. All tested electrodes were dismantled, rinsed with electrolyte solvent, and dried in a glove box before characterization.

Both Li–MnO_2 batteries and Li–O_2/lithium–air batteries were assembled by similar procedures to that described above for the synthesis of lithiated mesoporous MnO_2. To test the Li–MnO_2 cell performance, the battery was transferred to a sealed container flushed with argon. The Li–O_2 cell performance was tested after filling the container with oxygen. For dual applications of the cathode in Li–MnO_2 and lithium–air systems, the cell was first sealed with a gas-impermeable membrane, which was subsequently wiped off to enable air to enter the cell. The cell remained integrated during all these processes. Galvanostatic discharge–charge tests were carried out on a CT2001A battery-testing instrument (LAND Electronic Co.) at room temperature. Electrochemical impedance spectroscopy (EIS) was performed on a Parstat 2273 potentiostat/galvanostat workstation (AMETEK) at different charge–discharge states (open-circuit voltage: ca. 3.0 V, discharge voltage: ca. 2.4 V, recharge voltage: ca. 4.2 V) with an AC voltage of 10 mV in the frequency range of 100 kHz–100 mHz.

Keywords: electrocatalysis · Li–MnO_2 batteries · lithium–air batteries · manganese oxide · recycling

How to cite: *Angew. Chem. Int. Ed.* **2015**, *54*, 4338–4343
Angew. Chem. **2015**, *127*, 4412–4417

[1] a) *Lithium Ion Rechargeable Batteries* (Ed.: K. Ozawa), Wiley-VCH, Weinheim, **2009**; b) P. G. Bruce, B. Scrosati, J. M. Tarascon, *Angew. Chem. Int. Ed.* **2008**, *47*, 2930–2946; *Angew. Chem.* **2008**, *120*, 2972–2989.

[2] a) Y. S. Hu, Y. G. Guo, W. Sigle, S. Hore, P. Balaya, J. Maier, *Nat. Mater.* **2006**, *5*, 713–717; b) M. Winter, R. J. Brodd, *Chem. Rev.* **2004**, *104*, 4245–4270; c) M. V. Reddy, G. V. Subba Rao, B. V. R. Chowdari, *Chem. Rev.* **2013**, *113*, 5364–5457.

[3] a) E. Gratz, Q. Sa, D. Apelian, Y. Wang, *J. Power Sources* **2014**, *262*, 255–262; b) L. Li, L. Y. Zhai, X. X. Zhang, J. Lu, R. J. Chen, F. Wu, K. Amine, *J. Power Sources* **2014**, *262*, 380–385.

[4] a) Z. L. Jian, P. Liu, F. J. Li, P. He, X. W. Guo, M. W. Chen, H. S. Zhou, *Angew. Chem. Int. Ed.* **2014**, *53*, 442–446; *Angew. Chem.* **2014**, *126*, 452–456; b) T. Zhang, H. S. Zhou, *Nat. Commun.* **2013**, *4*, 1817–1823; c) H. D. Lim, H. Song, J. Kim, H. Gwon, Y. Bae, K. Y. Park, J. Hong, H. Kim, T. Kim, Y. H. Kim, X. Lepro, R. Ovalle-Robles, R. H. Baughman, K. Kang, *Angew. Chem. Int. Ed.* **2014**, *53*, 3926–3931; *Angew. Chem.* **2014**, *126*, 4007–4012; d) J. Lu, Y. Lei, K. C. Lau, X. Luo, P. Du, J. Wen, R. S. Assary, U. Das, D. J. Miller, J. W. Elam, H. M. Albishri, D. A. El-Hady, Y. K. Sun, L. A. Curtiss, K. Amine, *Nat. Commun.* **2013**, *4*, 2383–2391.

[5] a) Z. Q. Peng, S. A. Freunberger, Y. Chen, P. G. Bruce, *Science* **2012**, *337*, 563–566; b) B. D. McCloskey, R. Scheffler, A. Speidel, D. S. Bethune, R. M. Shelby, A. C. Luntz, *J. Am. Chem. Soc.* **2011**, *133*, 18038–18041; c) K. G. Gallagher, S. Goebel, T. Greszler, M. Mathias, W. Oelerich, D. Eroglu, V. Srinivasan, *Energy Environ. Sci.* **2014**, *7*, 1555–1563; d) K. Zhang, X. P. Han, Z. Hu, X. L. Zhang, Z. L. Tao, J. Chen, *Chem. Soc. Rev.* **2015**, *44*, 699–728.

[6] a) R. Merkle, J. Maier, *Angew. Chem. Int. Ed.* **2008**, *47*, 3874–3894; *Angew. Chem.* **2008**, *120*, 3936–3958; b) A. Débart, A. J. Paterson, J. Bao, P. G. Bruce, *Angew. Chem. Int. Ed.* **2008**, *47*, 4521–4524; *Angew. Chem.* **2008**, *120*, 4597–4600; c) L. Trahey, N. K. Karan, M. K. Y. Chan, J. Lu, Y. Ren, J. Greeley, M. Balasubramanian, A. K. Burrell, L. A. Curtiss, M. M. Thackeray, *Adv. Energy Mater.* **2013**, *3*, 75–84; d) K. L. Pickrahn, S. W. Park, Y. Gorlin, H. B. R. Lee, T. F. Jaramillo, S. F. Bent, *Adv. Energy Mater.* **2012**, *2*, 1269–1277; e) M. Bajdich, M. García-Mota, A. Vojvodic, J. K. Nørskov, A. T. Bell, *J. Am. Chem. Soc.* **2013**, *135*, 13521–13530.

[7] a) Y. Y. Shao, F. Ding, J. Xiao, J. Zhang, W. Xu, S. Park, J. G. Zhang, Y. Wang, J. Liu, *Adv. Funct. Mater.* **2013**, *23*, 987–1004; b) S. J. Guo, D. G. Li, H. Y. Zhu, S. Zhang, N. M. Markovic, V. R. Stamenkovic, S. H. Sun, *Angew. Chem. Int. Ed.* **2013**, *52*, 3465–3468; *Angew. Chem.* **2013**, *125*, 3549–3552; c) J. Lu, L. Li, J. B. Park, Y. K. Sun, F. Wu, K. Amine, *Chem. Rev.* **2014**, *114*, 5611–5640; d) Z. W. Chen, M. Waje, W. Z. Li, Y. S. Yan, *Angew. Chem. Int. Ed.* **2007**, *46*, 4060–4063; *Angew. Chem.* **2007**, *119*, 4138–4141; e) J. J. Xu, Z. L. Wang, D. Xu, L. L. Zhang, X. B. Zhang, *Nat. Commun.* **2013**, *4*, 2438.

[8] Z. Y. Lu, H. T. Wang, D. S. Kong, K. Yan, P. C. Hsu, G. Y. Zheng, H. B. Yao, Z. Liang, X. M. Sun, Y. Cui, *Nat. Commun.* **2014**, *5*, 4345.

[9] a) J. Park, H. Kim, K. Jin, B. J. Lee, Y. S. Park, H. Kim, I. Park, K. D. Yang, H. Y. Jeong, J. Kim, K. T. Hong, H. W. Jang, K. Kang, K. T. Nam, *J. Am. Chem. Soc.* **2014**, *136*, 4201–4211; b) D. M. Robinson, Y. B. Go, M. Greenblatt, G. C. Dismukes, *J. Am. Chem. Soc.* **2010**, *132*, 11467–11469; c) K. A. Stoerzinger, M. Risch, J. Suntivich, W. M. Lü, J. Zhou, M. D. Biegalski, H. M. Christen, Ariando, T. Venkatesan, Y. Shao-Horn, *Energy Environ. Sci.* **2013**, *6*, 1582–1588.

[10] a) F. Jiao, P. G. Bruce, *Adv. Mater.* **2007**, *19*, 657–660; b) J. Y. Luo, J. J. Zhang, Y. Y. Xia, *Chem. Mater.* **2006**, *18*, 5618–5623.

[11] a) H. L. Wang, Y. Yang, Y. Y. Liang, G. Y. Zheng, Y. G. Li, Y. Cui, H. J. Dai, *Energy Environ. Sci.* **2012**, *5*, 7931–7935; b) R. Choi, J. Jung, G. Kim, K. Song, Y. I. Kim, S. C. Jung, Y. K. Han, H. Song, Y. M. Kang, *Energy Environ. Sci.* **2014**, *7*, 1362–1368.

[12] H. Beyer, S. Meini, N. Tsiouvaras, M. Piana, H. A. Gasteiger, *Phys. Chem. Chem. Phys.* **2013**, *15*, 11025–11037.

[13] a) O. Gerbig, R. Merkle, J. Maier, *Adv. Mater.* **2013**, *25*, 3129–3133; b) M. Leskes, N. E. Drewett, L. J. Hardwick, P. G. Bruce, G. R. Goward, C. P. Grey, *Angew. Chem. Int. Ed.* **2012**, *51*, 8560–8563; *Angew. Chem.* **2012**, *124*, 8688–8691; c) F. Y. Cheng, J. Chen, *Chem. Soc. Rev.* **2012**, *41*, 2172–2192.

[14] J. Y. Luo, W. J. Cui, P. He, Y. Y. Xia, *Nat. Chem.* **2010**, *2*, 760–765.

[15] a) I. Roche, E. Chaînet, M. Chatenet, J. Vondrák, *J. Phys. Chem. C* **2007**, *111*, 1434–1443; b) W. Xiao, D. Wang, X. W. Lou, *J. Phys. Chem. C* **2010**, *114*, 1694–1700; c) J. Suntivich, H. A. Gasteiger, N. Yabuuchi, H. Nakanishi, J. B. Goodenough, Y. Shao-Horn, *Nat. Chem.* **2011**, *3*, 546–550; d) T. Takashima, K. Hashimoto, R. Nakamura, *J. Am. Chem. Soc.* **2012**, *134*, 1519–1527.

[16] a) D. A. Tompsett, S. C. Parker, M. S. Islam, *J. Am. Chem. Soc.* **2014**, *136*, 1418 – 1426; b) D. A. Tompsett, S. C. Parker, P. G. Bruce, M. S. Islam, *Chem. Mater.* **2013**, *25*, 536 – 541; c) C. Y. Ouyang, S. Q. Shi, M. S. Lei, *J. Alloys Compd.* **2009**, *474*, 370 – 374; d) T. A. Mellan, K. P. Maenetja, P. E. Ngoepe, S. M. Woodley, C. R. A. Catlow, R. Grau-Crespo, *J. Mater. Chem. A* **2013**, *1*, 14879 – 14887.

[17] a) K. P. C. Yao, Y. C. Lu, C. V. Amanchukwu, D. G. Kwabi, M. Risch, J. Zhou, A. Grimaud, P. T. Hammond, F. Bardé, Y. Shao-Horn, *Phys. Chem. Chem. Phys.* **2014**, *16*, 2297 – 2304; b) J. Suntivich, K. J. May, H. A. Gasteiger, J. B. Goodenough, Y. Shao-Horn, *Science* **2011**, *334*, 1383 – 1385.

Received: December 2, 2014
Published online: February 11, 2015

